Two Neighbouring Tunnels in Saturated Soil Under Blast Loading

Vladimir A. Osinov(✉) and Stylianos Chrisopoulos

Institute of Soil Mechanics and Rock Mechanics,
Karlsruhe Institute of Technology, 76128 Karlsruhe, Germany
{vladimir.osinov,stylianos.chrisopoulos}@kit.edu

Abstract. The paper deals with the numerical modelling of the blast-induced deformation of two neighbouring shallow tunnels and the surrounding soil. The deformation is caused by an explosion inside one of the tunnels. The explosion is simulated by a short-term pressure load of moderate amplitude (8 MPa) applied to the tunnel lining. The lining of both tunnels is circular with an inner diameter of 9.6 m and consists of concrete segments (tubbings) assumed to be linearly elastic. The tunnels are located at a depth of 17 m in fully saturated soil. The effective stresses in the soil are described by a hypoplasticity model. The modelling incorporates pore water cavitation at zero absolute pore pressure. The dynamic problem is solved in a two-dimensional plane-strain formulation with the finite-element program Abaqus/Standard. The transient deformation of the tunnel lining and the soil is analysed in detail. In particular, the solution reveals the emergence of large cavitation zones in the soil during the dynamic deformation.

1 Introduction

The problem of an explosion in a tunnel is a dynamic soil-structure interaction problem whose solution is determined by both the design of the structure (the tunnel lining) and the mechanical properties of the surrounding medium (soil, rock). The ground surface also plays an important role for shallow tunnels and should be included in the formulation of the problem. The modelling is usually aimed at finding the deformation and possible damage of the tunnel lining and neighbouring structures, e.g. an adjacent tunnel or a construction above the tunnel. If the tunnel is situated in saturated soil, an important question is that of the expected residual deformations and permanent stress changes in the soil. If the effective pressure in the soil is reduced to zero, the soil turns into a liquefaction state. Saturated soils can liquefy not only under cyclic shear deformation typical of earthquake-induced loading but also after large-amplitude compression-extension cycles [1,2].

This paper presents results of the numerical modelling of the dynamic deformation of two neighbouring tunnels and the surrounding saturated soil induced by an explosion inside one of the tunnels. Similar problems with a single tunnel

T. Triantafyllidis (Ed.): *Recent Developments of Soil Mechanics and Geotechnics in Theory and Practice*, LNACM 91, pp. 281–296, 2020.
https://doi.org/10.1007/978-3-030-28516-6_15

have been studied in [3,4]. The explosion is simulated by a short-term pressure load of moderate amplitude (8 MPa) applied to the tunnel lining. The lining of both tunnels is circular and consists of concrete segments (tubbings) assumed to be linearly elastic. The constitutive description of the soil is based on the effective-stress principle. The effective stresses are described by a hypoplasticity model for granular soils. The choice of a constitutive model for soil in problems with blast-induced deformation is dictated by the magnitude of the applied pressure. An increase in the effective pressure in a fully saturated soil under undrained conditions is a small fraction of the total pressure applied to the soil. For the loading considered in this paper, the transient effective-stress changes in the soil do not exceed a few hundred kilopascals and lie within the validity range of the hypoplasticity model. The constitutive description of the pore water includes cavitation with zero stiffness at zero absolute pore pressure and linearly elastic behaviour for a nonzero pressure.

The problem is solved with the finite-element program Abaqus/Standard in a two-dimensional plane-strain formulation. Although a real explosion originates from a point source and requires a three-dimensional formulation, an advantage of the two-dimensional formulation is that it enables us to solve the problem with fine spatial discretization. As pointed out in [3,4], problems with blast-induced soil deformation require finer spatial discretization than problems with quasi-static or earthquake-induced loading for the same geotechnical structure. Close inspection of the literature reveals that this requirement is often disregarded and the computational mesh is too coarse, especially for three-dimensional problems (for literature on the numerical modelling of blast-induced soil-structure interaction, see e.g. references in [5,6]). The necessary degree of spatial discretization depends on the spatial variation of the solution. Previous studies [3,4] as well as theoretical estimations show that, in order to obtain reliable numerical solutions, the grid spacing in a blast-induces soil-tunnel interaction problem should be as small as several centimetres. The present two-dimensional formulation allows us to obtain accurate solutions on a fine mesh and to analyse in detail the deformation of the tunnel lining and the soil.

2 Constitutive Description of the Soil

The total stress tensor in the soil is considered as the sum of the effective-stress tensor $\boldsymbol{\sigma}$ (compressive stresses are taken to be negative) and the isotropic tensor $-p_f\mathbf{I}$, where p_f is the pore pressure (positive for compression) and $\mathbf{I}$ is the unit tensor. The effective stress is described by a hypoplasticity model with intergranular strain proposed in [7] for cohesionless granular soils with rate independent behaviour. The model is an extension of an earlier version of hypoplasticity [8] and includes the intergranular-strain tensor as a new state variable in addition to the stress tensor and the void ratio. The constitutive equation gives the effective-stress rate $\dot{\boldsymbol{\sigma}}$ as a function of the strain rate $\dot{\boldsymbol{\varepsilon}}$, the effective-stress tensor $\boldsymbol{\sigma}$, the intergranular-strain tensor $\boldsymbol{\delta}$ and the void ratio e:

$$\dot{\boldsymbol{\sigma}} = \mathbf{H}\left(\dot{\boldsymbol{\varepsilon}}, \boldsymbol{\sigma}, \boldsymbol{\delta}, e\right). \tag{1}$$

The evolution of the intergranular-strain tensor is governed by the equation

$$\dot{\boldsymbol{\delta}} = \mathbf{F}\left(\dot{\boldsymbol{\varepsilon}}, \boldsymbol{\delta}\right). \tag{2}$$

For a detailed description of the functions **H** and **F** in (1), (2), see the original paper [7] or [9,10]. The constitutive parameters used in the present study are given in Tables 1 and 2.

Table 1. Constitutive parameters of Karlsruhe sand [11]

φ_c [°]	h_s [MPa]	e_{c0}	e_{d0}	e_{i0}	α	β	n
30	5800	0.84	0.53	1.0	0.13	1.0	0.28

Table 2. Additional constitutive parameters of the extended hypoplasticity model with intergranular strain [10]

R	m_R	m_T	β_r	χ
4×10^{-5}	5.0	5.0	0.05	1.5

The constitutive equation (1) is corrected at small stresses as described in [4]. The correction consists in the multiplication of the function **H** by a factor which depends on the mean stress. The correction has an effect on the constitutive response only at small stresses (below 1 kPa in absolute value). This small-stress correction, originally proposed in [12] for a different constitutive model, is used in order to avoid numerical problems caused by zero effective stress when the soil undergoes expansion. In the problem considered in this paper, large tensile deformations in the vertical direction are produced in the upper layer of dry soil after the reflection of the pressure wave from the free surface. With the correction factor introduced in (1), the mean stress in tension approaches zero asymptotically.

Assuming locally undrained conditions (zero soil permeability) and incompressible solid phase, the constitutive equation for the pore pressure reads

$$\dot{p_f} = -\frac{K_f}{n} \operatorname{tr} \dot{\boldsymbol{\varepsilon}}, \tag{3}$$

where K_f is the pore fluid bulk modulus, n is the porosity, and the deformation rate is negative for compression. In fully saturated soil, K_f is equal to the bulk modulus of pure water $K_w = 2.2$ GPa. If the soil undergoes tensile deformation and the absolute pore pressure (including the atmospheric pressure) becomes sufficiently low, the pore water begins to cavitate and the pore fluid bulk modulus abruptly falls to a nearly zero value. We assume that the pore water cannot withstand tensile stresses and that cavitation therefore begins at zero absolute pore pressure. If p_f^0 is the initial pore pressure in a soil element and ε_f is the

current volumetric strain of the pore fluid (zero at p_f^0), the pore fluid bulk modulus is

$$K_f = \begin{cases} K_w & \text{if} \quad \varepsilon_f < (p_f^0 + p_a)/K_w, \\ 0 & \text{if} \quad \varepsilon_f \geq (p_f^0 + p_a)/K_w, \end{cases} \tag{4}$$

where p_a is the atmospheric pressure (100 kPa). The volumetric strain of the pore fluid, ε_f, is equal to the volumetric strain of the soil, $\mathrm{tr}\,\boldsymbol{\varepsilon}$, divided by the porosity. Equation (4) produces a piecewise-linear strain-pressure dependence for the pore fluid as shown by the solid line in Fig. 1. The compression from a cavitated state with $p_f = -p_a$ is assumed to follow the same piecewise-linear curve.

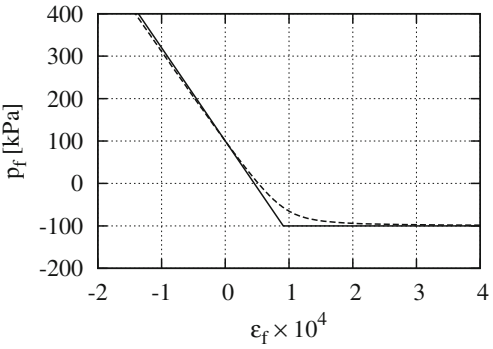

Fig. 1. Pore fluid pressure as a function of the pore fluid volumetric strain with $p_f^0 = 100$ kPa. Solid line: the function obtained with (4), dashed line: the smooth approximation

Figure 2 shows an example of uniaxial (oedometric) extension of saturated soil calculated with the hypoplasticity model for the soil skeleton. The kink on the total-stress curve shown by the solid line corresponds to the beginning of pore water cavitation according to (4). The total-stress curve for the compression from a cavitated state with $p_f = -p_a$ also has a kink at the point that corresponds to the closure of the voids in the pore water or, in terms of relation (4), at the point where $\varepsilon_f = (p_f^0 + p_a)/K_w$. The kink on the strain-stress curve due to pore water cavitation introduces a strong nonlinearity in the overall constitutive response of the soil in compression-extension in addition to the comparatively weak nonlinearity in the effective-stress response, see the curve for the effective stress in Fig. 2.

The strong nonlinearity in the compression from a cavitated to a fully saturated state is caused by a sharp increase in the soil stiffness at the moment when the cavitation voids in the pore water disappear. This increase has a substantial qualitative influence on the solutions of a dynamic problem. The increasing stiffness in combination with a high strain rate may lead to the formation of discontinuities (shock fronts) [13]. Examples related to a similar problem (an explosion in a tunnel) can be found in [3]. The shock fronts in [3] arise because of a small amount (few volume percent) of free gas in the soil and, as a consequence, the sharply increasing soil stiffness in compression. In the present study,

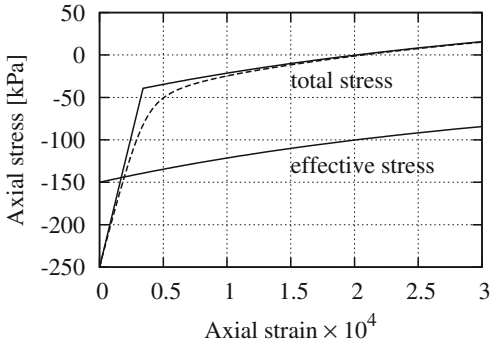

Fig. 2. Uniaxial extension of saturated soil calculated with the hypoplasticity model with a hydrostatic initial effective stress of −150 kPa, an initial pore pressure of 100 kPa and a void ratio of 0.6. Dashed line: the smooth approximation of pore water cavitation

along with the cavitation-related mechanism of shock formation, a shock front will also arise in the upper layer of dry soil where the mean stress will first be reduced to a nearly zero value during the wave reflection and then gradually restored during the subsequent compression. The increasing stiffness in compression will produce a shock front.

The formation and propagation of shock fronts make the numerical solution of a dynamic problem rather difficult, especially with commercial programs originally not intended to deal with discontinuous solutions. Besides the fact that problems with shock fronts require fine spatial discretization, they also require special means such as, for instance, viscous stresses. Otherwise the solution may be completely spoiled by spurious numerical oscillations. Viscous stresses with constant viscosity may not suffice: the oscillations may be eliminated, but at the cost of unrealistically high damping and the excessive smearing of the shock profile because of the too high viscosity. A more complicated approach may be needed to obtain satisfactory solutions.

In the present study, spurious oscillations in the numerical solutions are reduced by combining a smooth approximation of (4) and viscous stresses. First, the piecewise-linear strain-pressure relation for the pore pressure is approximated by a smooth curve as shown in Fig. 1 by the dashed line. The approximation is obtained by using the bulk modulus of a mixture of water and free gas instead of the modulus determined by (4). The smooth curve in Fig. 1 corresponds to the compression-extension of a mixture with an initial degree of saturation of 0.99999 at a pressure of 100 kPa. Second, viscous stresses are introduced in addition to the constitutive stresses (1) and the pore pressure. The values of the viscosity coefficients which produce satisfactory results have been found by trial and error. Constant viscosity coefficients turned out to be insufficient to achieve the desired effect for cavitation-induced shocks. The viscosity is made variable with a sharp increase during the transition of the pore fluid bulk modulus from zero to 2.2 GPa. For more detail, see [4].

3 Boundary-Value Problem

The boundary-value problem for two tunnels in a half-space is solved as a two-dimensional plane-strain problem shown in Fig. 3. The water table and the tunnel centres are located, respectively, at depths of 2 m and 17 m. The distance between the tunnel centres is 25 m. The tunnel lining is circular with an inner radius of 4.8 m. The lining is 0.45 m thick and consists of individual concrete tubbings as shown in Fig. 3. The tubbings and the concrete invert are modelled as linearly elastic materials. The tubbings are not bolted at the interfaces. The forces at the concrete-concrete and concrete-soil interfaces result from dry friction with a given friction angle. The parameters of the concrete and the friction angles are given in Table 3. The concrete-soil friction angle is taken to be zero because the contact algorithms available in Abaqus does not allow the user to model nonzero friction between concrete and saturated soil. The maximum shear stress at the contact surface is determined by the effective normal stress in the soil, whereas Abaqus uses the total normal stress when calculating the shear stress. The contact algorithms available in Abaqus can allow or forbid separation in the normal direction, depending on the user's choice. The problem is solved with separation for concrete-concrete interfaces and without separation for concrete-soil interfaces.

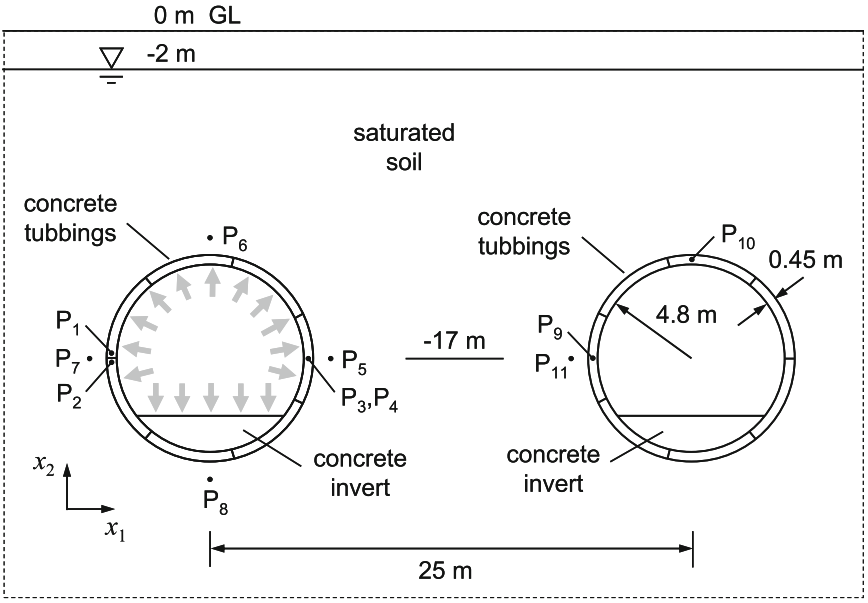

Fig. 3. Two tunnels in the half-space

Table 3. The concrete parameters and the friction angles

Young modulus [GPa]	40
Poisson ratio	0.2
Density [kg/m^3]	2400
Concrete-concrete friction angle [°]	45
Concrete-soil friction angle [°]	0

The initial stresses in the soil and in the tunnel lining are in static equilibrium with the gravity and are hydrostatic in the far field. The initial void ratio e is homogeneous and equal to 0.6. This corresponds to a relative density of 0.77 estimated as $(e_{c0} - e)/(e_{c0} - e_{d0})$, see Table 1. An explosion inside the left tunnel is simulated by a given pressure applied to the inner surface of the tunnel. The boundary condition for all points of the surface is shown in Fig. 4. The size of the computational domain is 250 m × 150 m. Transparent boundary conditions at the outer boundary are not used in the calculations. The type of boundary conditions at the outer boundary plays no role in this case, as the numerical solutions are valid only until the waves reflected from the outer boundary reach the domain of interest around the tunnels. The present computational domain enables us to model up to 120 ms.

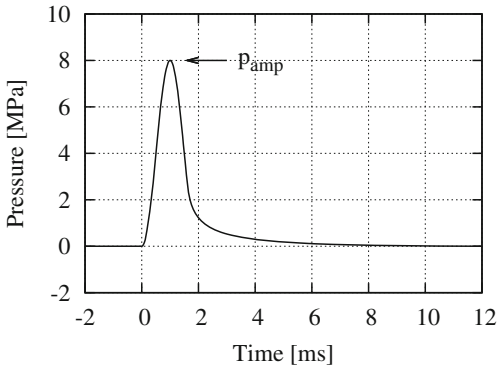

Fig. 4. Pressure applied to the inner surface of the tunnel

The boundary-value problem is solved with the finite-element program Abaqus/Standard with the implicit Hilber-Hughes-Taylor time integration scheme using the 4-node bilinear quadrilateral elements CPE4 with selectively reduced integration. The element size varies from about 6 cm in the tubbings and in the soil near the tunnels to 1 m near the outer boundary of the domain. The finite-element mesh near the lining is shown in Fig. 5. The time increment is 10^{-5} s.

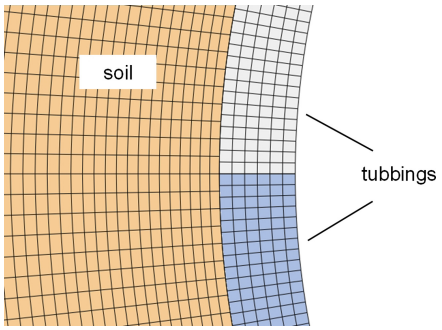

Fig. 5. Finite-element mesh near the lining

4 Deformation of the Lining

The pressure pulse shown in Fig. 4 is applied to the inner surface of the left tunnel. The motion of the tubbings can be traced by considering the displacements of two points P_1 and P_2 located in two neighbouring tubbings of the left tunnel near the contact surface between them as shown in Fig. 3. The displacement components at these points are shown in Fig. 6. The applied pressure causes the tubbings to move in the radial direction, see the curve for the horizontal displacement component u_1. Since the tubbings are not connected at the interface, their radial displacements result in the loss of contact between them at the beginning of the motion (in 1 ms), see two curves for the vertical component u_2. The maximum gap between the tubbings in this separation phase reaches 6 mm. The two curves for the vertical displacements also reveal high-frequency oscillations of the tubbings in the circumferential direction during the separation phase. The oscillations will be seen better from the stress curves below.

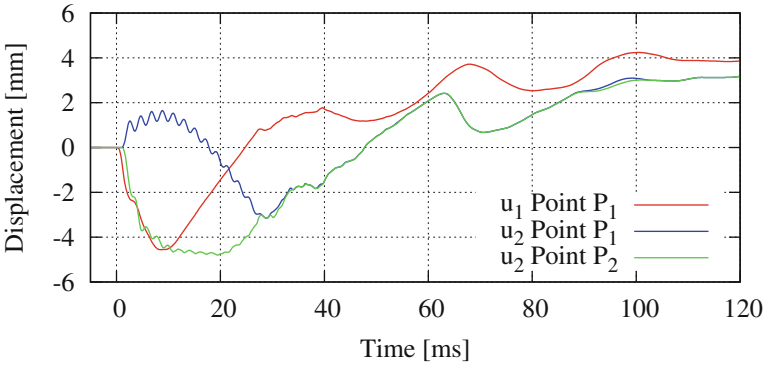

Fig. 6. Displacement components in the tubbings at points P_1 and P_2

The soil reaction decelerates the radial motion of the tubbings and then accelerates them in the opposite direction to the tunnel centre until the contact between them is restored again. As seen from Fig. 6, the separation phase lasts 27 ms. The duration of the separation phase may differ by few milliseconds for different pairs of tubbings. The maximum radial displacement of the tubbings during the separation phase is 4.5 mm, see the curve for u_1 in Fig. 6.

In order to trace the stresses induced in the tunnel lining during its deformation, consider two points P_3 and P_4 located, respectively, near the free surface and near the concrete-soil interface in the middle part of the tubbing, see Fig. 3. The circumferential stress component at points P_3 and P_4 is shown in Fig. 7. The curves in the figure reveal high-frequency oscillations of the tubbing in the circumferential direction during the separation phase mentioned above. The oscillations arise in the form of a standing wave with a frequency of 480 Hz. The frequency depends on the tubbing length in the circumferential direction and would be higher for shorter tubbings as is the case, for instance, in [4]. The maximum tensile and compressive stresses during the oscillations are, respectively, 15 and 12 MPa. These values are greater than the pressure applied to the lining (8 MPa). Since the oscillations occur in the form of a standing wave, the stress amplitude varies along the tubbing: it is maximal in the middle part and vanishes near the ends.

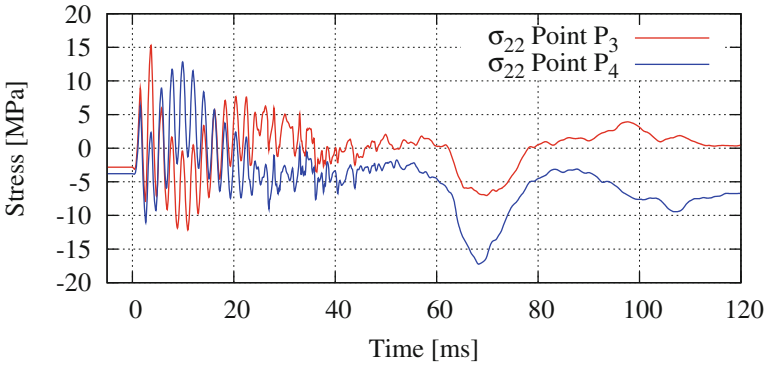

Fig. 7. Circumferential stresses in the lining of the left tunnel at points P_3 and P_4 located, respectively, near the free surface and near the concrete-soil interface

The closure of the gaps between different pairs of tubbings at the end of their separation phases is not simultaneous. The tubbings collisions during the nonsimultaneous closure induce irregular oscillations of the circumferential stress in the interval between 25 and 50 ms observed in Fig. 7. In the time between 60 and 80 ms, the curves in Fig. 7 show a relatively slow loading-unloading cycle with a high compressive stress between 7 and 17 MPa. This indicates that the whole lining is subjected to an external pressure. The cause of this pressure will be evident from the analysis of the soil deformation in the next Section.

The pressure pulse applied to the lining of the left tunnel is transmitted to the soil and transforms into a pressure wave. The wave propagates in the soil and compresses the lining of the right tunnel leading to an increase in the compressive circumferential stresses in the tubbings and a few oscillations of the lining as a whole. This is seen from Fig. 8 which shows the circumferential stresses at points P_9 and P_{10} in the tubbings of the right tunnel. The maximum increase in the compressive stresses is about 7 MPa. Neither tensile stresses nor separation of the tubbings are observed in the lining of the right tunnel.

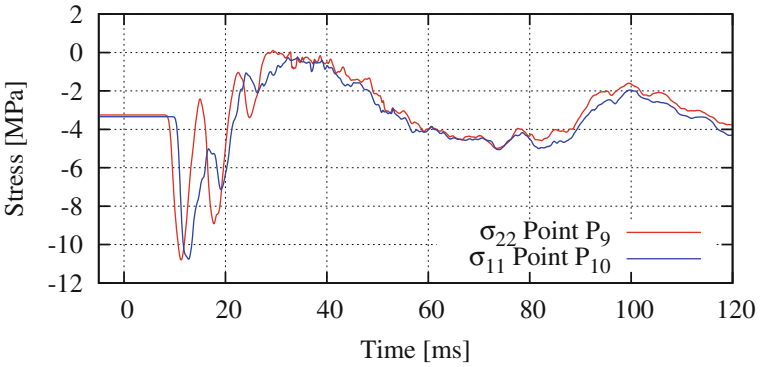

Fig. 8. Circumferential stresses in the lining of the right tunnel at points P_9 and P_{10}

5 Deformation of the Soil

The loading applied to the tunnel lining induces a complicated dynamic process in which the soil is subjected to both compressive and tensile deformation. The tensile deformation turns out to be large enough to reduce the absolute pore pressure to zero and thus to give rise to pore water cavitation. Recall that the transition to cavitation in this study is approximated by a smooth curve, see Fig. 1, so that zero absolute pressure is reached asymptotically and the onset of cavitation becomes undefined. However, for the analysis of solutions it is convenient to distinguish between cavitated and noncavitated water. In order to be able to identify a cavitation zone, we say that the pore water is cavitated if the pore pressure p_f is below -99 kPa.

The pore pressure distribution in the soil at different times is shown in Figs. 9, 10. The cavitation begins in three distinct places: near the upper half of the lining of the left tunnel, beneath the upper layer of dry soil and near the right tunnel. The cavitation around the left tunnel begins after 7 ms, yet before the top tubbings reach their maximum radial displacement. The cavitation beneath the dry soil layer arises at nearly the same time when the pressure wave (red colour in Fig. 9 for $t = 11$ ms) reaches this layer. If the half-space were linearly elastic, the reflected wave would have a tensile stress of the same order of magnitude as

in the incident pressure wave. The interaction of a high-pressure wave with the ground surface in saturated soil is more complicated and has much in common with the reflection of high-pressure waves from the free surface in water. In both cases, tensile stresses are limited to 100 kPa (zero effective stress in the soil skeleton and zero absolute pore pressure assumed as a threshold for pore water cavitation). As a consequence, the interaction of the blast-induced pressure wave with the ground surface in the soil results in the formation of a cavitation zone instead of a reflected wave with high tensile stresses. The third cavitation zone near the right tunnel arises at a later time when the pressure wave passes around the tunnel and interacts with the tunnel lining, see Fig. 9 for $t = 11$ ms. The interaction leads to the wave reflection with large tensile deformations and pore water cavitation. The mechanism is similar to that of the reflection from the ground surface.

The three emerging cavitation zones grow in size, coalesce and form one big cavitation zone as seen in Fig. 9 for $t = 16$ and 26 ms. As the upper tubbings of the left tunnel come into contact with each other at the end of the separation phase, they stop the radial motion of the adjacent soil. The cavitated pore water in the soil is compressed to a noncavitated state, and the cavitation boundary moves upwards from the lining into the soil. At the same time, the upper boundary of the cavitation zone moves downwards, leading to the shrinkage of the cavitation zone as well. The shrinkage of the cavitation zone is a complicated process with highly nonlinear soil behaviour in compression near the boundary of the zone, see Figs. 1, 2 for the one-dimensional uniaxial case. In particular, Fig. 10 for $t = 56$ ms reveals singularities with high pressure gradients at the ends of the narrow cavitation zone at the final stage of its shrinkage.

The closure of the cavitation zone produces a spreading high-pressure zone with pressures of up to 1.5 MPa and two pressure waves, one of which propagates upwards and the other one downwards, see Fig. 10 for $t = 62$ ms. The wave that propagates upwards is reflected from the upper soil layer in the same manner as the primary blast-induced pressure wave and produces a new smaller cavitation zone, Fig. 10 for $t = 70$ ms. The wave that propagates downwards passes around the tunnel, deforms the tunnel lining and increases the circumferential stresses in the tubbings in the time between 60 and 80 ms as we have seen in Fig. 7.

The time dependence of the volumetric strain and the mean effective stress in the soil is shown in Figs. 11, 12 at four points P_5, P_6, P_7, P_8 around the left tunnel and at point P_{11} near the right tunnel. The points are located at a distance of 1 m from the tunnel, see Fig. 3. The blast-induced pressure wave produces a short compression-extension cycle followed by a longer extension-compression cycle. The latter coincides with the cavitation phase, except for point P_8 where no cavitation is observed. An analysis of the individual strain components reveals that the principal axes of the strain tensor rotate, making the deformation path rather complicated. Figure 12 shows that the mean effective stress in the soil is substantially reduced. The residual effective stress is difficult to predict, as it depends, besides the loading amplitude, on many factors such as the constitutive behaviour of the skeleton, the pore fluid compressibility and the

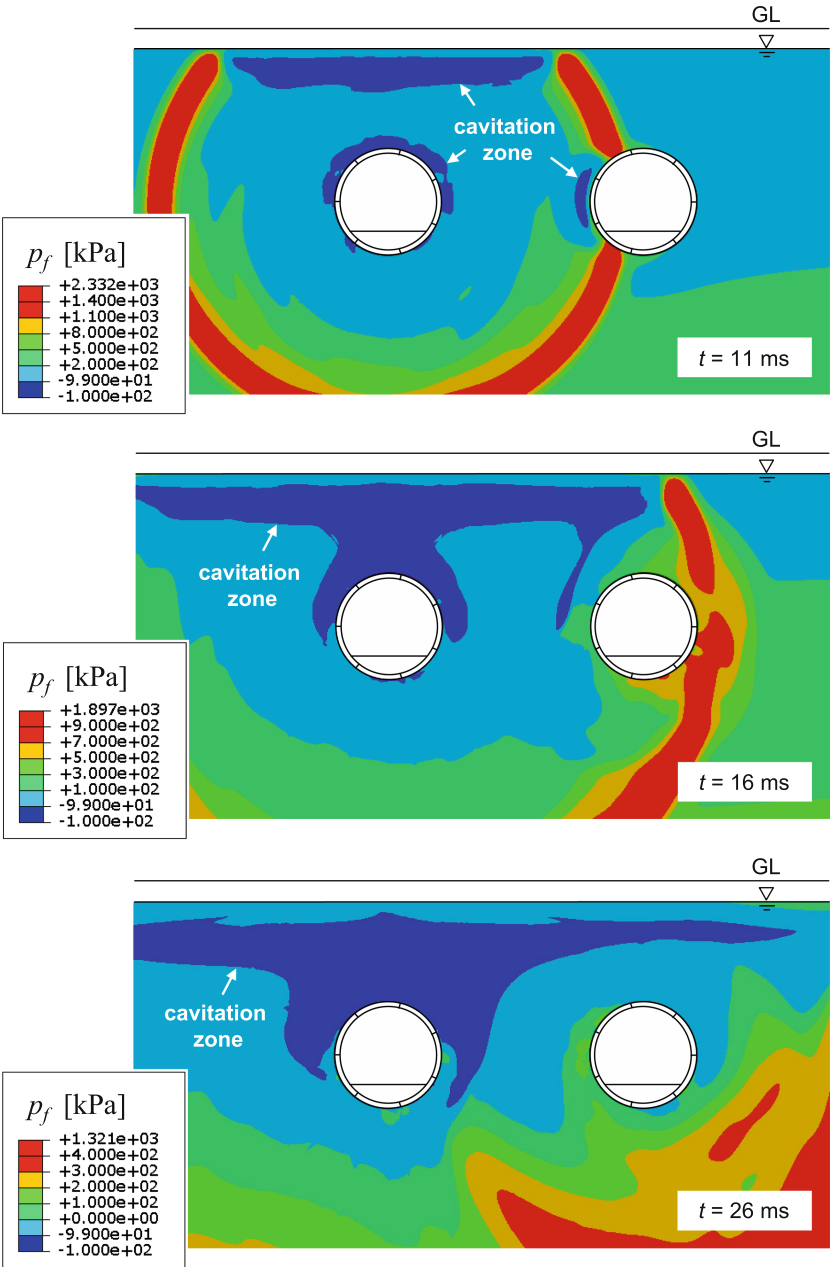

Fig. 9. Pore pressure in the soil at different times

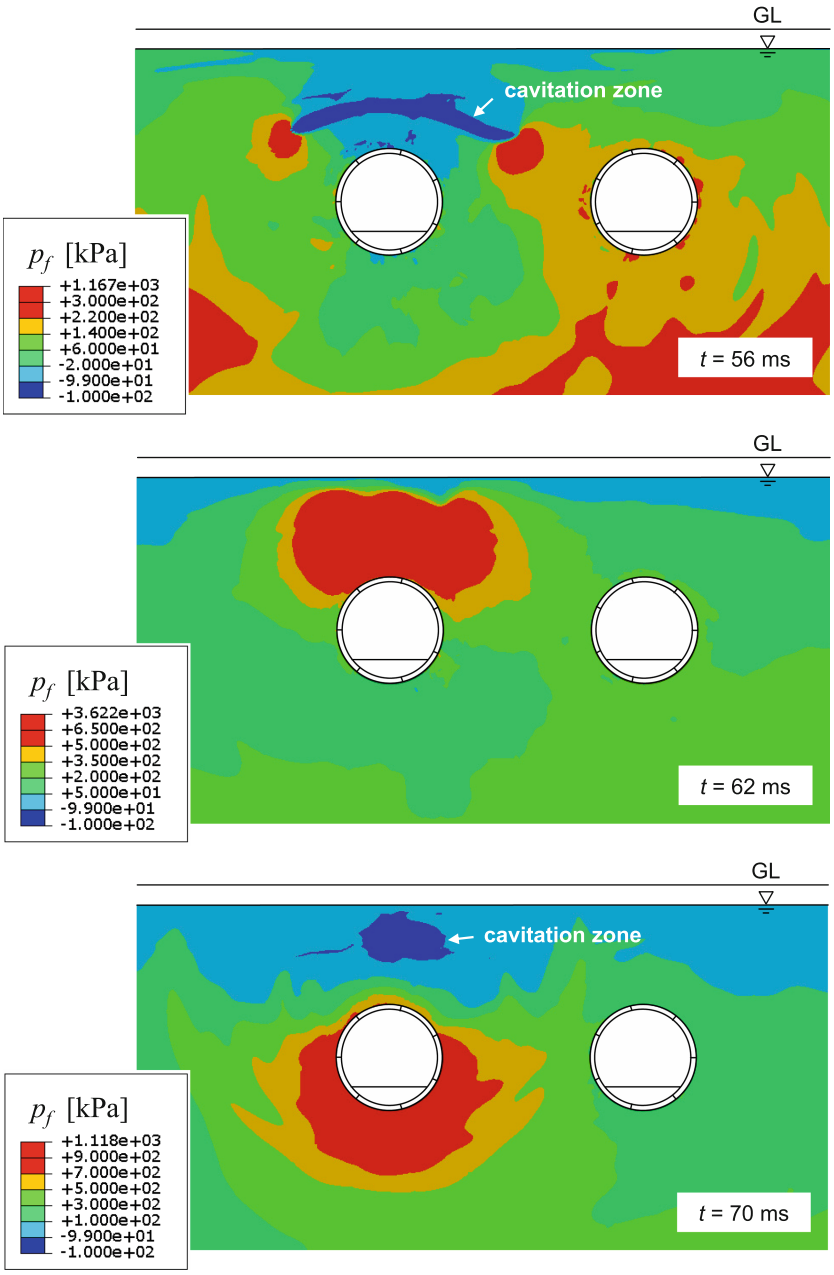

Fig. 10. Pore pressure in the soil at different times

initial stress state. Deformation paths like those in Fig. 11 with sufficiently large compression and extension amplitudes can eventually lead to the reduction of the effective stress to zero and to momentary soil liquefaction [1,2]. This may happen not only at higher loading amplitudes but also in the case of a small amount of free gas in the pore water, which results in higher pore fluid compressibility and, as a consequence, in a larger strain during the compression phase [3].

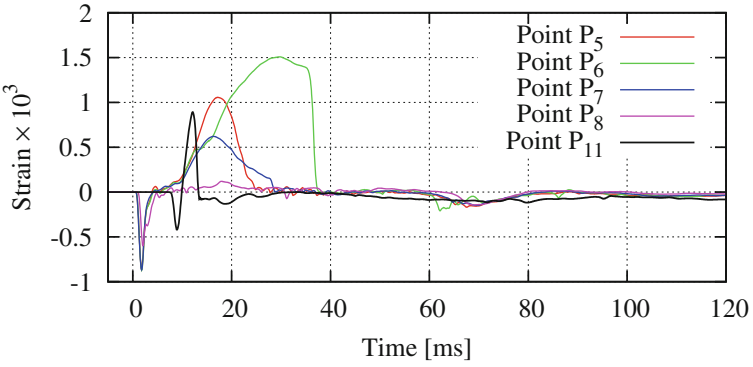

Fig. 11. Volumetric strain in the soil at different points

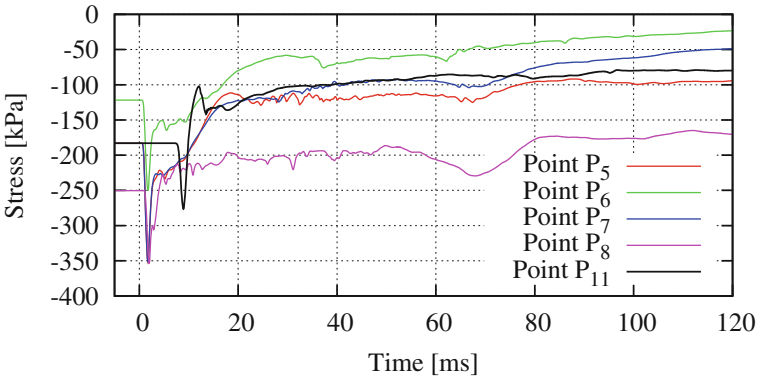

Fig. 12. Mean effective stress in the soil at different points

The motion of the soil does not end after 120 ms covered by the present numerical solution. This is seen in Fig. 13 which shows the vertical displacement components at three points in the soil above the left tunnel. The first two points lie in the upper layer of dry soil.

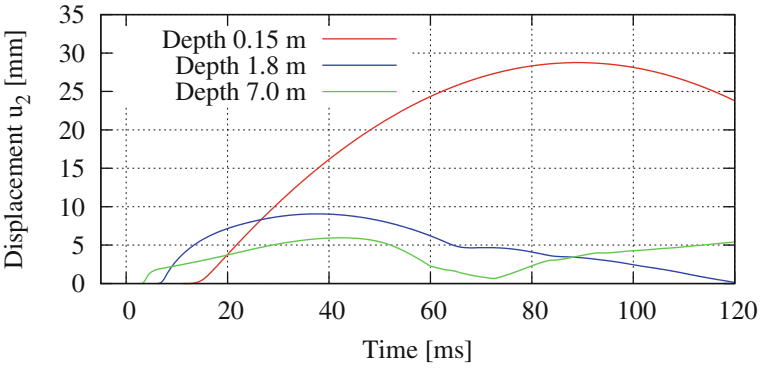

Fig. 13. Vertical displacement of the soil above the left tunnel

In order to assess the influence of the adjacent tunnel, the present problem has also been solved with a single tunnel. A comparison of the two solutions in the vicinity of the tunnel up to a few metres from the lining shows that the influence of the adjacent tunnel is insignificant.

6 Conclusion

The main features of the blast-induced deformation of the tunnel lining and the soil can be summarized as follows. The tubbings of the tunnel subjected to blasting lose contact with each other after 1 ms and are in a separation phase during the next 25–28 ms (Fig. 6). The maximum radial displacement and the maximum gap between the tubbings in the separation phase are of the order of several millimetres. The tubbings exhibit high-frequency oscillations (480 Hz) during the separation phase, with the maximum tensile and compressive oscillating stresses being by 50–80% greater than the blast pressure applied to the lining (Fig. 7).

The numerical solution shows an important role of pore water cavitation in the deformation process. The soil expansion following the blast-induced pressure wave is large enough to give rise to pore water cavitation (Fig. 9, $t = 11$ ms). A big cavitation zone forms after 15 ms between the tunnels and the ground surface (Fig. 9, $t = 16$ and 26 ms). The volumetric soil stiffness sharply increases in the transition from a cavitated state back to full saturation, making the strain-pressure relation highly nonlinear (Figs. 1, 2). As a consequence, the shrinkage of the cavitation zone is accompanied by high gradients (shock fronts) and singularities at the boundaries of the cavitation zone (Fig. 10, $t = 56$ ms). The ultimate closure of the cavitation zone produces a high-pressure domain which in turn induces two pressure waves (Fig. 10, $t = 62$ and 70 ms).

The complexity of the deformation paths makes it difficult to predict permanent changes in the effective pressure in the soil. The qualitative conclusion is that the effective pressure in the vicinity of both tunnels may be considerably reduced (Fig. 12). The largest decrease is observed above the tunnel subjected to blasting.

References

1. Fragaszy, R.J., Voss, M.E.: Undrained compression behavior of sand. J. Geot. Eng. ASCE **112**(3), 334–347 (1986)
2. Bolton, J.M., Durnford, D.S., Charlie, W.A.: One-dimensional shock and quasi-static liquefaction of silt and sand. J. Geot. Eng. ASCE **120**(10), 1874–1889 (1994)
3. Osinov, V.A.: Blast-induced waves in soil around a tunnel. Arch. Appl. Mech. **81**, 543–559 (2011)
4. Osinov, V.A., Chrisopoulos, S., Triantafyllidis. Th.: Numerical analysis of the tunnel-soil interaction caused by an explosion in the tunnel. Soil Dyn. Earthq. Eng. **122**, 318-326 (2019)
5. Feldgun, V.R., Karinski, Y.S., Yankelevsky, D.Z.: The effect of an explosion in a tunnel on a neighboring buried structure. Tunn. Undergr. Space Technol. **44**, 42–55 (2014)
6. Lu, G., Fall, M.: A coupled chemo-viscoplastic cap model for simulating the behavior of hydrating cemented tailings backfill under blast loading. Int. J. Numer. Anal. Meth. Geomech. **40**, 1123–1149 (2016)
7. Niemunis, A., Herle, I.: Hypoplastic model for cohesionless soils with elastic strain range. Mech. Cohesive-frict. Mater. **2**(4), 279–299 (1997)
8. von Wolffersdorff, P.A.: A hypoplastic relation for granular materials with a predefined limit state surface. Mech. Cohesive-frict. Mater. **1**(3), 251–271 (1996)
9. Osinov, V.A.: Large-strain dynamic cavity expansion in a granular material. J. Eng. Math. **52**, 185–198 (2005)
10. Osinov, V.A., Gudehus, G.: Dynamics of hypoplastic materials: theory and numerical implementation. In: Hutter, K., Kirchner, N. (eds.) Dynamic Response of Granular and Porous Materials under Large and Catastrophic Deformations, pp. 265–284. Springer, Berlin (2003)
11. Herle, I., Gudehus, G.: Determination of parameters of a hypoplastic constitutive model from properties of grain assemblies. Mech. Cohesive-frict. Mater. **4**, 461–486 (1999)
12. Osinov, V.A., Chrisopoulos, S., Grandas-Tavera, C.: Vibration-induced stress changes in saturated soil: a high-cycle problem. In: Triantafyllidis, T. (ed.) Holistic Simulation of Geotechnical Installation Processes. Benchmarks and Simulations, pp. 69–84. Springer, Cham (2016)
13. Osinov, V.A.: Longitudinal shock waves in soil (this volume)